Modern Valence-Bond Description of Chemical Reaction Mechanisms: The 1,3-Dipolar Addition of Methyl Azide to Ethene

Joshua J. Blavins and Peter B. Karadakov*

Department of Chemistry, University of York, Heslington, York YO10 5DD, U.K.

David L. Cooper

Department of Chemistry, University of Liverpool, Liverpool L69 7ZD, U.K.

Received: October 29, 2002; In Final Form: February 4, 2003

Spin-coupled [SC(8)/6-31G(d,p)] calculations on top of the MP2/6-31G(d,p) intrinsic reaction coordinate are used in order to obtain a model for the electronic mechanism of the gas-phase concerted 1,3-dipolar cycloaddition (13DC) reaction between methyl azide (CH_3N_3) and ethene (C_2H_4). It is shown that this reaction follows a homolytic mechanism characterized by an almost simultaneous breaking of the two coplanar π bonds in methyl azide and of the π bond in ethene, and the subsequent reengagement of the valence orbitals initially responsible for these bonds into two new bonds, closing the triazole ring, and a lone pair on the central nitrogen in the product. This is in contrast to previous SC research which established heterolytic mechanisms, realized through the movement of electron pairs, for 13DC reactions involving 1,3-dipoles with more polar coplanar π bonds, such as fulminic acid (HCNO) and diazomethane (CH_2N_2). We find that neither the homolytic nor heterolytic mechanisms for 13DC reactions involve aromatic transition states. Other aspects of the gas-phase concerted 13DC reaction of methyl azide with ethene, including optimized transition structure geometry, electronic activation energy, activation barrier corrected for zero-point energies, and standard enthalpy, entropy, and Gibbs free energy of activation, have been calculated at the HF/6-31G(d), HF/6-31G(d,p), B3LYP/6-31G(d), B3LYP/6-31G(d,p), MP2/6-31G(d), MP2/6-31G(d,p), QCISD/6-31G(d), and CCD/6-31G(d) levels of theory. The paper includes a critical survey of recently published research on the electronic mechanisms of 13DC reactions and reveals the limitations of approaches relying on closed-shell wave functions and/or on hand-crafted valence-bond constructions.

1. Introduction

The mechanisms of 1,3-dipolar cycloaddition (13DC) reactions have been a long-standing source of controversy among theoretical and experimental chemists. One side of the dispute, now largely resolved, relates to the synchronicity of 13DC reactions and can be traced back to the works of Huisgen,[1,2] who suggested that these reactions proceed through a synchronous concerted mechanism, and of Firestone,[3,4] who put forward an alternative stepwise biradical pathway. High-level ab initio calculations support the synchronous concerted mechanism and predict activation barriers within the correct experimental range[5,6] (for a detailed account of pre-1988 theoretical work, and further references, see the review by Borden et al.[7]).

More recently, the nature of the electronic rearrangements taking place during 13DC reactions (see the reaction mechanisms below) has come under the spotlight. The extent of disagreement between the results of different authors is sufficient to justify a short critical discussion which will set the grounds for the research reported in the present paper.

An approach which is particularly suitable for the study of electronic reaction mechanisms is a modern form of valence-bond (VB) theory, the spin-coupled (SC) method.[8,9] In our previous work, SC wave functions were used to follow and interpret the electronic structure reorganizations along the

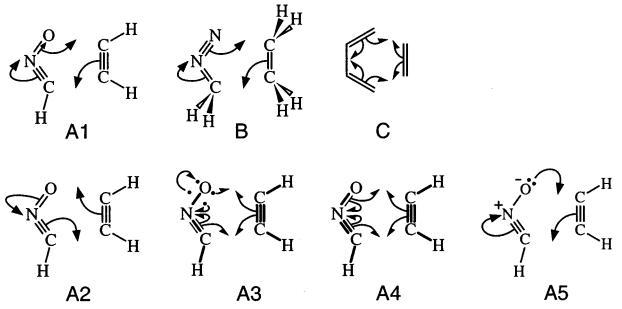

reaction paths for the 13DC reactions between fulminic acid and ethyne ($HCNO + C_2H_2$),[10] and between diazomethane and ethene ($CH_2N_2 + C_2H_4$).[11] Both reactions were found to progress through practically identical heterolytic mechanisms, characterized by the movement of three well-identifiable orbital pairs that are retained along the entire reaction path from reactants to product (see reaction mechanisms A1 and B; note that as indicated by the N to O arrow in reaction mechanism A1, the corresponding N−O π bond is strongly polarized toward the oxygen atom). When applied to pericyclic reactions, SC theory can predict not only heterolytic mechanisms such as A1 and B, but also homolytic electronic structure rearrangements, in which bonds (or corresponding orbital pairs) in the reactants break and the orbitals participating in these bonds reengage in the new bonds present in the product. One example is provided by the SC description of the Diels−Alder reaction[12] which can be

* To whom correspondence should be addressed. E-mail: pbk1@york.ac.uk.

10.1021/jp027331d CCC: $25.00
Published on Web 03/15/2003

represented by reaction mechanism C, where the half-arrows illustrate the changes in the bonding pattern between the six SC orbitals forming the active space. It is important to emphasize that in most of the existing applications to pericyclic reactions, a SC wave function incorporating a single product of *N* nonorthogonal singly occupied active orbitals accounts for more than 90% of the correlation energy of a "*N* in *N*" complete active-space self-consistent field (CASSCF) wave function over the whole reaction path; the overlap between SC and CASSCF wave functions is also very high (often above 0.99). Just as in the case of an "*N* in *N*" CASSCF wave function, the only two elements of the SC wave function which are specified externally are the size of the active space (number of SC orbitals) and the type of the AO basis. In this way, the choice between a heterolytic or homolytic mechanism is not made ad hoc, but by the fully variational procedure used to optimize the SC wave function. This flexibility is not shared by all quantum chemical approaches used to describe chemical reactions: The single-configuration closed-shell wave function used in the restricted Hartree−Fock (RHF) method and restricted density-functional theory (RDFT) is inherently incapable of accommodating a homolytic mechanism. Even in cases when the SC treatment indicates a heterolytic mechanism, there can be important differences from the uncorrelated RHF picture: For example, in the case of the 13DC reaction between fulminic acid and ethyne, both the SC and RHF[13,14] treatments support reaction mechanism A1. However, in the case of the 13DC reaction involving diazomethane and ethene, our SC analysis results in reaction mechanism B, while RHF theory[13,15,16] suggests an electron flow in the opposite direction (i.e., of the type illustrated by reaction mechanism A2).

A different mechanism for the 13DC reaction between fulminic acid and ethyne (see reaction mechanism A2) was suggested by Nguyen et al.[17] These authors made use of two approaches, the first of which (CI-LMO-CAS) involves localization of the "6-in-5" CASSCF active-space orbitals and analysis of the weights of configurations expressed in terms of these localized orbitals. However, the two configurations used to derive the reaction mechanism are far from dominating the CASSCF wave function: Their combined weight never exceeds ca. 44%. Furthermore, the particular choice of the active space requires one of the active orbitals to be doubly occupied, and one would naturally expect this doubly occupied orbital to be localized about one of the more electronegative atoms, O or N, which provides a plausible explanation of a preference for the electron transfer in reaction mechanism A2. The second approach involves calculating DFT-based reactivity descriptors for fulminic acid. The utility of approaches of this type is limited by the fact that, as a rule, these treat an isolated reactant molecule, which is not only unable to "feel" the influence of other reactants but also has an equilibrium geometry that can be very different from its conformation near the transition state (TS). This last is particularly evident in the case of fulminic acid, as the gas-phase equilibrium geometry of the isolated molecule is linear.

A qualitative classical VB analysis carried out by Harcourt[18] led to the formulation of a "concerted biradical" mechanism for 13DC reactions (see also ref 19 and refs 7, 8, and 11 therein). Although this combination of terms may sound unusual to those dealing with pericyclic reactions (as a rule, within the accepted terminology "biradical mechanism" is synonymous with a nonconcerted, stepwise mechanism involving a biradical intermediate), in this instance "biradical" was used to denote a homolytic electronic rearrangement. In a more recent paper, Harcourt and Schulz[20] discussed possible homolytic mechanisms for the 13DC reaction between fulminic acid and ethyne. Their ideas are illustrated by reaction mechanisms A3 and A4. The dots on the two sides of the O−N bond in reaction mechanism A3 represent singly occupied π_x(ON) and π_y(ON) localized molecular orbitals (LMOs), while the thick and thin lines in both A3 and A4 reflect Harcourt's notation for normal and fractional electron-pair bonds, respectively. According to Harcourt and Schulz, the reaction mechanism to be preferred is A3. The presence of LMOs of π symmetry in this reaction mechanism is a giveaway for the fact that the analyses of reaction mechanisms A3 and A4 in ref 20 are based on the electronic structure of HCNO at its linear gas-phase equilibrium geometry and do not take into account the presence of the second reactant and the changes in the geometry of the reacting system along the reaction path. As a rule, the wave functions used by Harcourt and co-workers are molecule-specific, carefully hand-crafted classical VB constructions which are defined within a minimal set of basis functions. Wave functions of this type cannot ordinarily be used to provide a consistent picture of electronic structure changes along a general reaction path, as such hand tuning is likely to require different wave function constructions at different points along this path. Harcourt and Schulz have criticized reaction mechanism A1 (and, effectively, mechanism A2) stating that this mechanism should involve charge transfer between the species. This is not correct: The 13DC reaction between fulminic acid and ethyne is a concerted, almost synchronous process and so all electron rearrangements depicted by reaction mechanisms A1 and A2 take place simultaneously, without any noticeable charge transfer between the reactants. Although the terms "heterolytic" and "homolytic" are used to distinguish between mechanisms A1 and C, these do not imply the existence of any biradical or zwitterionic intermediates (see ref 12).

Sakata[21] carried out a HF-level population analysis along the reaction path of the 13DC reaction between fulminic acid and ethyne. His results suggest reaction mechanism A5, which is very similar to mechanism A1 and in line with previous HF-level results.

Nguyen et al. have recently published a comment[22] on the existing models for the electronic mechanism of the HCNO + C_2H_2 13DC reaction which has prompted two replies.[19,23] In that comment, despite the substantial differences between the types of VB approach in refs 12 and 20 (see above), the contrast between the predictions following from the two very different treatments (compare mechanism A1 to mechanisms A3 and A4) has been used to cast a shade of doubt over the credibility of any VB-theory-based analysis of the electronic structure rearrangements during 13DC reactions. In fact, although the results of SC calculations indicate the heterolytic mechanisms A1 and B for the 13DC reactions between fulminic acid and ethyne, and diazomethane and ethene, respectively, there is nothing that would prevent SC theory from predicting homolytic mechanisms for other 13DC reactions. For example, expanding on an argument presented by Harcourt,[19] due to symmetry reasons the ozonolysis of ethene should proceed through a homolytic mechanism within any approach which is sufficiently flexible to allow a mechanism of this type. The reacting systems corresponding to real-world 13DC reactions rarely have any symmetry, but it would be reasonable to expect that homolytic mechanisms could be observed in 13DC reactions in which the bonds in the 1,3-dipole and dipolarophile that break during the reaction are essentially nonpolar.

In the present paper we carry out SC calculations along the reaction path of the gas-phase 13DC reaction between methyl azide (CH_3N_3) and ethene and show that this reaction follows a homolytic mechanism. In addition to a model for the electronic reaction mechanism, SC theory can furnish important information about the nature of the TS. As a rule, the SC descriptions of pericyclic reactions that follow homolytic mechanisms indicate that the corresponding transition states may be considered aromatic,[12,24] while reactions proceeding through heterolytic mechanisms pass through nonaromatic transition states.[10,11] The TS in the 13DC reaction between methyl azide and ethene is shown to be nonaromatic and provides our first example of a TS of this type that occurs in conjunction with a homolytic mechanism. One interesting feature of this TS is that one can associate a nonneglible amount of singlet biradical character with the methyl azide fragment, which is all but absent from the SC description of the isolated 1,3-dipole.

2. Computational Procedure

In a nutshell, the SC model for the electronic mechanism of a chemical reaction is obtained in two steps: First, we use an existing efficient implementation of a high-level molecular orbital method in order to optimize the transition structure and a sequence of geometries along the minimum energy path[25,26] (also known as the intrinsic reaction coordinate, IRC[27,28]) in the directions of reactant(s) and product(s). This is followed by SC calculations at selected geometries along the IRC and the analysis of the results of such calculations.

The selection of the approach used to determine the evolution of the geometry of the reacting system is important, but not overly so: Faithful reproduction of the main qualitative features in the regions of bond-breaking and bond-formation is usually sufficient, as the shapes of the SC orbitals and the associated spin-coupling pattern are relatively insensitive to small conformational changes. In principle, the best option would be to employ a many-body perturbation theory treatment based on a CASSCF reference, such as CASPT2,[29] CASPT2N,[30] or CASMP2,[31] but the current unavailability of analytic gradients for any of these approaches all but precludes their use in TS optimizations and IRC calculations. Left with the choice between CASSCF and approaches utilizing a HF reference wave function, such as Møller−Plesset perturbation theory (MP*n*), coupled-cluster with doubles (CCD), or quadratic configuration interaction including single and double substitutions (QCISD), we decided to use the latter, plus DFT (B3LYP). This choice ensures proper inclusion of dynamic correlation effects, which, as shown by Borden and Davidson,[32] can be essential for the proper description of pericyclic reactions. We did not experience any SCF convergence difficulties in any of the HF and DFT calculations reported in the present paper, and it is reasonable to assume that all the reacting system geometries we have studied are within the limits of applicability of the closed-shell ansatz. Our choice is further supported by the fact that, in a previous ab initio study of the influence of solvent effects on the 13DC reaction between methyl azide and ethene, Repasky and Jorgensen[33] also used closed-shell wave functions [HF with 6-31G(d), 6-31+G(d), 6-311+G(d), 6-311+G(d,p), and 6-311+G(2df,2p) basis sets, and B3LYP/6-31G(d)] and reached the conclusion that the geometry of the TS for this concerted, almost synchronous process is not much affected by basis set extension beyond 6-31G(d) or by the use of B3LYP rather than HF.

The geometries of the concerted TS, the reactants (methyl azide and ethene) and of the product (4,5-dehydro-1-methyl-1*H*-[1,2,3]triazole) were optimized at the HF/6-31G(d), HF/6-31G(d,p), B3LYP/6-31G(d), B3LYP/6-31G(d,p), MP2/6-31G-(d), MP2/6-31G(d,p), QCISD/6-31G(d), and CCD/6-31G(d) levels of theory. Additionally, the TS was optimized using a MP4(SDQ)/6-31G(d) construction. It is interesting to mention that a number of attempts to optimize the geometry of the larger reactant, methyl azide, using the same approach, either did not converge or resulted in a first-order saddle point. The intrinsic reaction coordinate (IRC) was calculated at the MP2/6-31G(d,p) level of theory, starting from the corresponding TS, for 20 steps of 0.1 amu$^{1/2}$ bohr, both in the direction of the reactants and in the direction of the product. All geometry optimizations and the IRC calculation were performed using GAUSSIAN98[34] subject to the default convergence criteria. The MP*n*, QCISD, and CC wave functions used in this paper incorporate the default GAUSSIAN98 "frozen-core" (FC) approximation. All optimized TS geometries were shown to be first-order saddle points on the corresponding energy hypersurfaces through diagonalization of analytic (HF, B3LYP, and MP2) or numerical [QCISD, CCD, and MP4(SDQ)] Hessians calculated at these geometries.

Ordinarily, 13DC reactions are considered to be of the [π4s + π2s] type, where four electrons come from the π system of the 1,3-dipole and the remaining two from the dipolarophile. This suggests that the minimum number of active orbitals within the active space of a SC (or CASSCF) wave function used to describe such a 13DC reaction is six. SC wave functions with six active orbitals [SC(6)] have been found to be completely adequate for the descriptions of the electronic reaction mechanisms of the 13DC reactions of fulminic acid to ethyne[10] and of diazomethane to ethene.[11] However, initial attempts to use a SC(6) wave function, in the case of the 13DC reaction of methyl azide with ethene, met with difficulties at IRC geometries close to that of the product. Just as in a standard CASSCF calculation, the core and active orbitals within the SC wave function represent general MO expansions in terms of a suitable basis of atomic orbitals (AOs) contributed by all atoms in the system. The core and active orbitals (and the active-space spin function, see below) are optimized simultaneously, without any ad hoc restrictions except for the fixed number of active orbitals. The flexibility of the wave function creates possibilities for undesirable redistributions of the active and core orbitals during the optimization process which may lead to lower energy solutions, in which the active orbitals are no longer associated with the bonds and lone pairs directly involved in the chemical reaction. Following the changes of the electronic structure of the reacting system for the 13DC reaction of methyl azide with ethene along the IRC into the region near the product, two of the active SC orbitals would be expected to form a lone pair on the central nitrogen atom. However, the SC(6) calculation produces a lower-energy solution, in which this lone pair is described by a doubly occupied orbital, and two active orbitals shift to the almost π N−N bond. To prevent this change in the six-orbital active space, while retaining a fully variational wave function, we decided to carry out the SC analysis of the electronic mechanism of the 13DC reaction of methyl azide with ethene using a SC wave function with eight active orbitals, in which the two additional orbitals are initially engaged in the second almost π N−N bond in methyl azide.

The SC(8) wave function used to describe the electronic structure of the reacting system can be written in the form

$$\Psi_{00}^{8} = \hat{\mathcal{A}}[(\prod_{i=1}^{19}\varphi_i\alpha\,\varphi_i\beta)(\prod_{\mu=1}^{8}\psi_\mu)\Theta_{00}^{8}] \qquad (1)$$

in which φ_i and ψ_μ stand for the doubly occupied core (or,

inactive) and singly occupied nonorthogonal active (or, spin-coupled) orbitals, respectively. Θ^8_{00} denotes the normalized eight-electron active-space spin function

$$\Theta^8_{00} = \sum_{k=1}^{14} C_{0k}\Theta^8_{00;k} \tag{2}$$

which is allowed to be a most general linear combination of all 14 unique spin-coupling schemes $\Theta^8_{00;k}$ for a singlet system of eight electrons. The zero subscripts in Θ^8_{00} and $\Theta^8_{00;k}$ indicate the values of the total spin S and its z-projection M. The spin-coupling coefficients C_{0k} (these are optimized together with the active and core orbitals) do not depend on M and so the single zero subscript reflects the value of S.

SC calculations were carried out at the MP2/6-31G(d,p) TS geometry of the reacting system and at selected points along the corresponding IRC using the methodology described in ref 36. All one- and two-electron integrals in the 6-31G(d,p) basis required by the SC code were evaluated using the GAMESS-US program package.[37]

When analyzing an overall active-space spin-coupling pattern such as Θ^8_{00} in eq 2, it is often convenient to switch between different (full) sets of spin eigenfunctions (in the case of an eight-electron singlet, a full set consists of all 14 $\Theta^8_{00;k}$). The most useful sets of spin eigenfunctions have proven to be those introduced by Kotani, Rumer, and Serber (for a detailed discussion of the construction and properties of spin eigenfunctions, see ref 38). Although the code used to carry out the SC calculations reported in the present paper works in the Kotani spin basis, it is more convenient to discuss the changes in the active-space spin-coupling pattern during the 13DC reaction of methyl azide with ethene if Θ^8_{00} is expressed in terms of the Rumer spin basis. The required transformation can be carried out in a straightforward manner with the use of a specialized code for symbolic generation and manipulation of spin eigenfunctions (SPINS, see ref 39).

Each of the Rumer spin eigenfunctions ${}^{\mathrm{R}}\Theta^8_{00;1}-{}^{\mathrm{R}}\Theta^8_{00;14}$ represents a product of four singlet two-electron spin functions:

$$\begin{aligned}
&{}^{\mathrm{R}}\Theta^8_{00;1} \equiv (1\text{-}2,3\text{-}4,5\text{-}6,7\text{-}8), \quad {}^{\mathrm{R}}\Theta^8_{00;2} \equiv (1\text{-}4,2\text{-}3,5\text{-}6,7\text{-}8)\\
&{}^{\mathrm{R}}\Theta^8_{00;3} \equiv (1\text{-}2,3\text{-}6,4\text{-}5,7\text{-}8), \quad {}^{\mathrm{R}}\Theta^8_{00;4} \equiv (1\text{-}6,2\text{-}3,4\text{-}5,7\text{-}8)\\
&{}^{\mathrm{R}}\Theta^8_{00;5} \equiv (1\text{-}6,2\text{-}5,3\text{-}4,7\text{-}8), \quad {}^{\mathrm{R}}\Theta^8_{00;6} \equiv (1\text{-}2,3\text{-}4,5\text{-}8,6\text{-}7)\\
&{}^{\mathrm{R}}\Theta^8_{00;7} \equiv (1\text{-}4,2\text{-}3,5\text{-}8,6\text{-}7), \quad {}^{\mathrm{R}}\Theta^8_{00;8} \equiv (1\text{-}2,3\text{-}8,4\text{-}5,6\text{-}7)\\
&{}^{\mathrm{R}}\Theta^8_{00;9} \equiv (1\text{-}8,2\text{-}3,4\text{-}5,6\text{-}7), \quad {}^{\mathrm{R}}\Theta^8_{00;10} \equiv (1\text{-}8,2\text{-}5,3\text{-}4,6\text{-}7)\\
&{}^{\mathrm{R}}\Theta^8_{00;11} \equiv (1\text{-}2,3\text{-}8,4\text{-}7,5\text{-}6), \quad {}^{\mathrm{R}}\Theta^8_{00;12} \equiv (1\text{-}8,2\text{-}3,4\text{-}7,5\text{-}6)\\
&{}^{\mathrm{R}}\Theta^8_{00;13} \equiv (1\text{-}8,2\text{-}7,3\text{-}4,5\text{-}6), \quad {}^{\mathrm{R}}\Theta^8_{00;14} \equiv (1\text{-}8,2\text{-}7,3\text{-}6,4\text{-}5)
\end{aligned} \tag{3}$$

The pairs of numbers within the brackets indicate the indices of the electrons engaged in the singlet two-electron spin functions. For example, the complete expression for the first Rumer spin function, also known as the "perfect-pairing" (PP) spin function, is given by

$$\begin{aligned}
{}^{\mathrm{R}}\Theta^8_{00;1} &\equiv (1\text{-}2,3\text{-}4,5\text{-}6,7\text{-}8)\\
&= (1/4)[\alpha(1)\beta(2) - \alpha(2)\beta(1)] \times\\
&\quad [\alpha(3)\beta(4) - \alpha(4)\beta(3)][\alpha(5)\beta(6) - \alpha(6)\beta(5)] \times\\
&\quad [\alpha(7)\beta(8) - \alpha(8)\beta(7)]
\end{aligned} \tag{4}$$

The graphical representation of Rumer functions involves Rumer diagrams, which have much in common with the resonance structures drawn in standard organic chemistry textbooks. As shown in Figure 1, the Rumer diagrams for a singlet system of eight electrons fall in three distinct groups: If we use an analogy with the resonance structures for cyclooctatetraene, the first group resembles structures with π bonds only between adjacent carbons, while the second and third groups contain diagrams which are in one-to-one correspondence with structures with one and two para π bonds, respectively.

In many cases, the analogy between Rumer diagrams and resonance structures allows a straightforward translation of the results of SC calculations into classical VB terms. The Rumer spin basis is nonorthogonal and so the weights of the individual spin functions within Θ^8_{00} (see eq 2) cannot be calculated by simply taking the squares of the spin-coupling coefficients C_{0k}. Two frequently used weighting expressions are those suggested by Chirgwin and Coulson,[40] and by Gallup and Norbeck.[41] In the case of an eight-electron singlet active-space spin function expanded in the Rumer spin basis these expressions can be written as

$${}^{\mathrm{R}}P^{8,\mathrm{CC}}_{0k} = {}^{\mathrm{R}}C_{0k}\sum_{l=1}^{14}\langle {}^{\mathrm{R}}\Theta^8_{00;k}|{}^{\mathrm{R}}\Theta^8_{00;l}\rangle {}^{\mathrm{R}}C_{0l} \tag{5}$$

$${}^{\mathrm{R}}P^{8,\mathrm{GN}}_{0k} = c\,{}^{\mathrm{R}}C^2_{0k}/(\langle {}^{\mathrm{R}}\boldsymbol{\Theta}^8_{00}|{}^{\mathrm{R}}\boldsymbol{\Theta}^8_{00}\rangle^{-1})_{kk},$$
$$(c^{\mathrm{R}})^{-1} = \sum_{k=1}^{14} {}^{\mathrm{R}}C^2_{0k}/(\langle {}^{\mathrm{R}}\boldsymbol{\Theta}^8_{00}|{}^{\mathrm{R}}\boldsymbol{\Theta}^8_{00}\rangle^{-1})_{kk} \tag{6}$$

where $\langle {}^{\mathrm{R}}\boldsymbol{\Theta}^8_{00}|{}^{\mathrm{R}}\boldsymbol{\Theta}^8_{00}\rangle$ stands for the overlap matrix between the Rumer spin functions defined in eq 3.

A disadvantage of the more popular Chirgwin−Coulson formula is that it does not guarantee that all of the weights will lie in the range 0−1: When Θ^8_{00} is strongly dominated by a single Rumer spin function, the weight of this mode can exceed one, while, to compensate for this, other weights would have to be (small) negative numbers.

To verify that the SC(8) wave function incorporates most of the correlation effects within the active space spanned by the SC orbitals, we also performed "eight electrons-in-eight orbitals" SCVB calculations, at selected points along the MP2/6-31G(d,p) IRC using core and valence orbitals taken from the corresponding SC(8) wave functions. The full "8-in-8" SCVB wave function constructed from these orbitals (which are not reoptimized) takes the form of a linear combination of all structures in which none, or one to four of the active orbitals can be doubly occupied:

$${}^{\mathrm{SCVB}}\Psi^8_{00} = \sum_{K=1}^{1764} C_{0K}\Psi^8_{00;K} \tag{7}$$

$$\Psi^8_{00;K} \equiv \Psi^8_{00;k}(\mu_1\mu_2...\mu_{8-\nu}) = \hat{\mathcal{A}}[(\prod_{i=1}^{19}\varphi_i\alpha\ \varphi_i\beta)(\prod_{j=1}^{\nu}\psi_{\mu_j}\alpha\ \psi_{\mu_j}\beta)(\prod_{j=\nu+1}^{8-\nu}\psi_{\mu_j})\Theta^{8-2\nu}_{00;k}] \tag{8}$$

The number ν in $\Psi^8_{00;k}(\mu_1\mu_2...\mu_{8-\nu})$ can vary between 0 and 4,

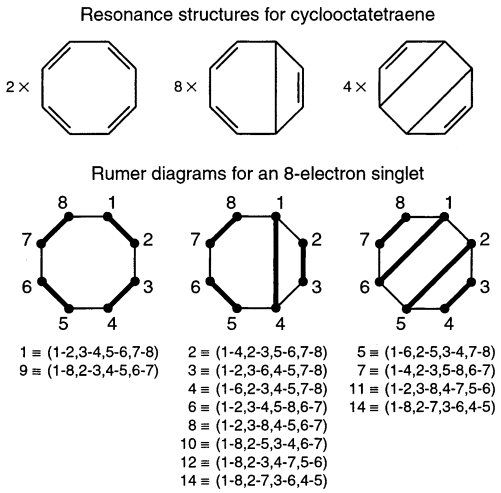

Figure 1. Resonance structures for cyclooctatetraene and Rumer diagrams for an eight-electron singlet system.

giving rise to covalent, singly, doubly, triply, and quadruply ionic structures. Of course, the list of configurations included in ${}^{\mathrm{SCVB}}\Psi^8_{00}$ coincides with that of an "8-in-8" CASSCF wave function. If these two wave functions are constructed with a common set of frozen core orbitals, then experience suggests that they should be very similar to one another, with only small differences arising from the slightly different spaces spanned by the two sets of active orbitals. An accurate estimate of these differences was provided by an additional CASSCF(8,8)/6-31G(d,p)//MP2/6-31G(d,p) calculation at the TS carried out by means of MOLPRO.[35]

As an alternative to eq 1, it is possible to represent the SC-(8) wave function as a linear combination of the 14 covalent structures,

$$\Psi^8_{00} = \sum_{k=1}^{14} C_{0k}\Psi^8_{00;k}(12345678) \tag{9}$$

The relative importance of the structures making up the SC-(8) and full-SCVB(8) wave functions which, in general, are nonorthogonal, can be established, for example, by means of Chirgwin−Coulson occupation numbers similar to those in eq 5,

$$P^{8,\mathrm{CC}}_{0K} = C_{0K}\sum_L \langle\Psi^8_{00;K}|\Psi^8_{00;L}\rangle C_{0L} / \sum_{K,L} C_{0K}\langle\Psi^8_{00;K}|\Psi^8_{00;L}\rangle C_{0L} \tag{10}$$

The full-SCVB(8) calculations were performed using code that implements the theory presented in ref 42 and which works in the Rumer spin basis.

In the present paper we also include a SC description of the electronic structure of the larger reactant (methyl azide) obtained with a SC(6) wave function

$$\Psi^6_{00} = \hat{\mathscr{A}}[(\prod_{i=1}^{12}\varphi'_i\alpha\ \varphi'_i\beta)(\prod_{\mu=1}^{6}\psi'_\mu)\Theta^6_{00}] \tag{11}$$

where $\Theta^6{}_{00}$ stands for the $S = 0$, $M = 0$ six-electron active-space spin function

$$\Theta^6_{00} = \sum_{k=1}^{5} C_{0k}\Theta^6_{00;k} \tag{12}$$

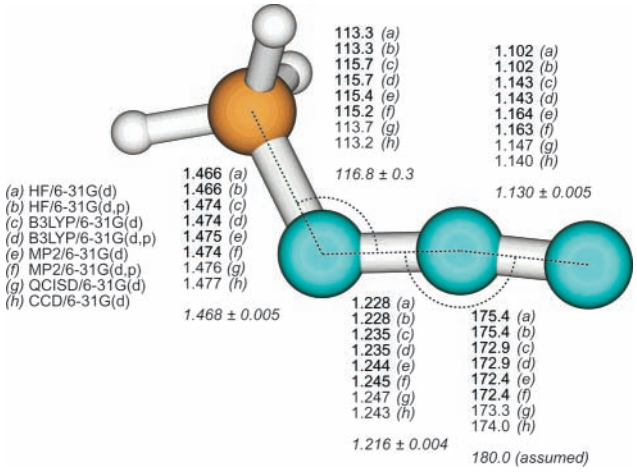

Figure 2. Equilibrium geometry of CH_3N_3 optimized at different levels of theory. Gas-phase electron diffraction values (bottom numbers in each column, in italics) from ref 45. Bond lengths in angstroms, angles in degrees.

Within the Rumer spin basis, Θ^6_{00} can be expanded in terms of the following five unique singlet six-electron spin eigenfunctions, each of which represents a product of three singlet two-electron spin functions:

$${}^{\mathrm{R}}\Theta^6_{00;1} \equiv (1\text{-}2,3\text{-}4,5\text{-}6), \quad {}^{\mathrm{R}}\Theta^6_{00;2} \equiv (1\text{-}4,2\text{-}3,5\text{-}6)$$

$${}^{\mathrm{R}}\Theta^6_{00;3} \equiv (1\text{-}2,3\text{-}6,4\text{-}5), \quad {}^{\mathrm{R}}\Theta^6_{00;4} \equiv (1\text{-}6,2\text{-}3,4\text{-}5)$$

$${}^{\mathrm{R}}\Theta^6_{00;5} \equiv (1\text{-}6,2\text{-}5,3\text{-}4) \tag{13}$$

3. Results and Discussion

Previous SC studies of 1,3-dipoles[43,44] have treated fulminic acid (HCNO), nitrone (CH_2NHO), diazomethane (CH_2N_2), and the triatomics N_2O, O_3, and NO_2, but (apparently) no azides. Although we did not expect the SC description of methyl azide to hold any major surprises, it was interesting to see whether the use of a larger active space (6 vs 4 SC orbitals) and the presence of the methyl substituent would cause any noticeable deviation from the established SC model of such systems.

The more important structural parameters of the CH_3N_3 C_s equilibrium geometry, optimized at different levels of theory, are indicated in Figure 2. The HF/6-31G(d) and B3LYP/6-31G(d,p) numbers are identical to those reported by Repasky and Jorgensen[33] and, as was observed by those authors, we find that extension of the 6-31G(d) basis, in our case to 6-31G(d,p), has a negligible effect on the optimized geometries. The results obtained using different methods exhibit relatively small variations, with the exception of the shorter of the two N−N bond lengths, for which the HF and MP2 estimates differ by ca. 0.06 Å. This is not surprising, as the experimental bond length of 1.130 Å suggests that this is very much a triple bond (the experimental N−N bond length in gaseous N_2 is 1.098 Å) and its proper description would require inclusion of electron correlation effects that are overestimated within the MP2 ansatz.

The shapes of the spin-coupled orbitals from the SC(6)/6-31G(d,p)//MP2/6-31G(d,p) wave function for methyl azide are shown in Figure 3, and the corresponding orbital overlaps are listed in Table 1. It is straightforward to see that the SC orbitals of A'' symmetry, $\psi'_1-\psi'_4$, are engaged in a bonding pattern strongly reminiscent of those in other 1,3-dipoles,[43,44] which involves two very similar, essentially nonpolar N−N π bonds, between orbitals ψ'_1 and ψ'_2, and ψ'_3 and ψ'_4, respectively. The

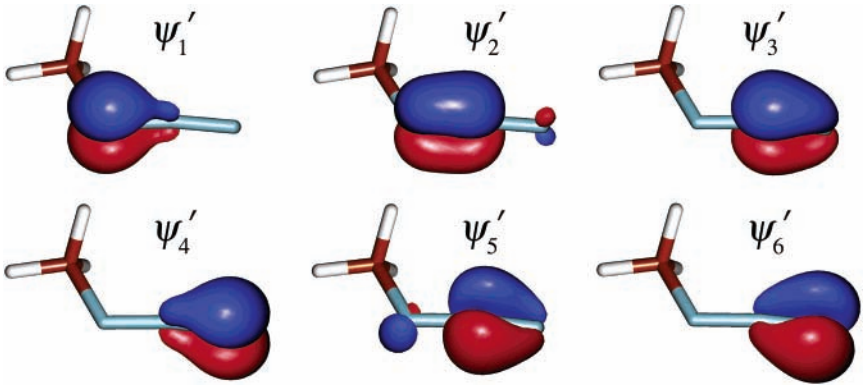

Figure 3. Active (valence) orbitals ψ_1',ψ_2',...,ψ_6' from the SC(6) wave function for methyl azide. Three-dimensional isovalue surfaces corresponding to $\psi_\mu' = \pm 0.1$, drawn from virtual reality modeling language (VRML) files produced by MOLDEN.[46]

TABLE 1: Overlap Integrals between the SC Orbitals from the SC(6)/6-31G(d,p)//MP2/6-31G(d,p) Wavefunction for Methyl Azide

	ψ_1'	ψ_2'	ψ_3'	ψ_4'	ψ_5'	ψ_6'
ψ_1'	1	0.755	0.224	0.140	0	0
ψ_2'		1	0.554	0.076	0	0
ψ_3'			1	0.709	0	0
ψ_4'				1	0	0
ψ_5'					1	0.663
ψ_6'						1

TABLE 2: Chirgwin−Coulson ($^{R}P_{0k}^{6,CC}$) and Gallup−Norbeck ($^{R}P_{0k}^{6,GN}$) Weights of the Rumer Spin Functions Included in the Active Space Spin-coupling Pattern Θ_{00}^{6} for Methyl Azide[a]

k	spin function	$^{R}P_{0k}^{6,CC}$	$^{R}P_{0k}^{6,GN}$
1	(1-2,3-4,5-6)	0.817	0.922
2	(1-4,2-3,5-6)	0.066	0.023
3	(1-2,3-6,4-5)	0.109	0.054
4	(1-6,2-3,4-5)	0.001	0.000
5	(1-6,2-5,3-4)	0.007	0.000

[a] See eqs 11 and 12.

two remaining SC orbitals, ψ_5' and ψ_6', which are of A' symmetry, form an additional π bond between the central and terminal nitrogens. This picture is reinforced by the fact that the active-space spin-coupling pattern (see Table 2) is heavily dominated by the PP spin function, (1-2,3-4,5-6), in which the spins of the three pairs of orbitals forming π bonds are coupled to singlets. The description of the electronic structure of methyl azide contained within the SC(6) wave function can be represented with the diagram

$$H_3C-N{=}N{\equiv}N$$

Similarly to SC theory findings for other 1,3-dipoles, the central nitrogen atom in methyl azide is "hypervalent" or "hypercoordinate", in the sense that it is connected to its neighbors through more than four covalent bonds: a double bond with a π component described by the orbital pair (ψ_1', ψ_2') and a triple bond with π components realized by the orbital pairs (ψ_3', ψ_4') and (ψ_5', ψ_6').

Previous SC studies of molecules incorporating multiple bonds[47] have revealed the presence of nonnegligible "resonance" between different ways of coupling the spins of the valence orbitals involved in the multiple bond. To a smaller degree, a "resonance" of this type is also observed within the SC(6) description of CH_3N_3. The second most important Rumer spin function (1-2,3-6,4-5) retains the singlet coupling between the SC orbitals associated with the N=N bond (ψ_1', ψ_2'), but

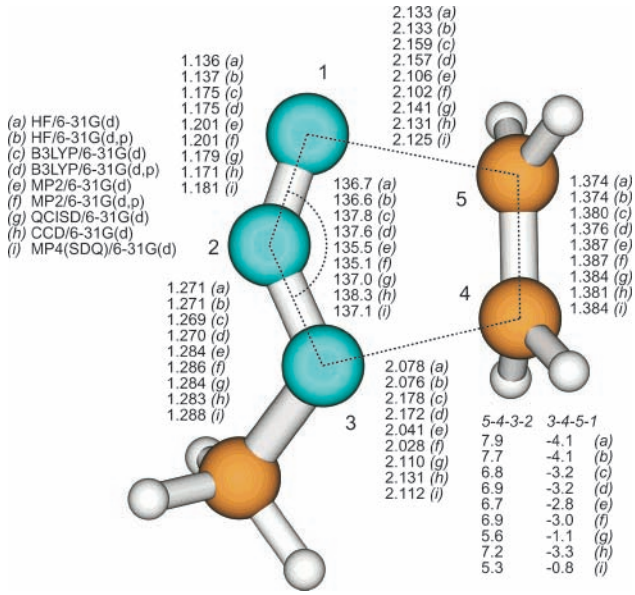

Figure 4. Geometry of the TS for the gas-phase 13DC reaction of methyl azide with ethene, optimized at different levels of theory. Bond lengths in angstroms, angles in degrees.

switches partners within the singlet pairs of SC orbitals from the N≡N bond: These now involve orbitals ψ_3' and ψ_6', and ψ_4' and ψ_5', respectively. With the progress of the 13DC reaction between methyl azide and ethene, the CH_3N_3 fragment loses its plane of symmetry, which leads to more pronounced interactions between the four SC orbitals which were initially responsible for the two π components of the N≡N bond. This provides a further justification for the use of an eight-orbital, rather than a six-orbital, active space for the description of the reaction mechanism.

The data presented in Figure 4 allows comparison between the main features of the concerted TS geometries for the 13DC reaction of methyl azide with ethene, optimized at different levels of theory. Repeating the observations made when discussing the equilibrium geometry of CH_3N_3 (see above), the HF/6-31G(d) and B3LYP/6-31G(d,p) bond lengths and angles are virtually identical to those reported in ref 33, and once again, we find that augmentation of the 6-31G(d) basis with a set of H p functions has only a minor effect on the optimized geometries. The differences between the HF and MP2 values for the N≡N bond length noted in CH_3N_3 are carried over to the TS. The lengths of the forming C−N bonds show that B3LYP suggests a slightly "earlier" TS in comparison to MP2, while the predictions of all other approaches fall between the MP2 and B3LYP estimates. The values for the two dihedral

TABLE 3: Electronic Activation Energies ($\Delta^{\ddagger}E_{elec}$) and Activation Barriers Including Zero-Point Energy Corrections [$\Delta^{\ddagger}(E_{elec} + ZPE)$], and the Standard (Taken as 298.15 K, 1 atm) Enthalpies ($\Delta^{\ddagger}H^{\ominus}$), Entropies ($\Delta^{\ddagger}S^{\ominus}$), and Gibbs Free Energies of Activation ($\Delta^{\ddagger}G^{\ominus}$) for the Gas-Phase 13DC Reaction of Methyl Azide with Ethene and for the Cycloelimination of Ethene from 4,5-Dehydro-1-methyl-1*H*-[1,2,3]triazole (Values in Parentheses)[a]

method	$\Delta^{\ddagger}E_{elec}$	$\Delta^{\ddagger}(E_{elec} + ZPE)$	$\Delta^{\ddagger}H^{\ominus}$	$\Delta^{\ddagger}S^{\ominus}$	$\Delta^{\ddagger}G^{\ominus}$
HF/6-31G(d)	38.5(71.2)	40.4(67.0)	39.2(67.6)	−40.6(4.7)	51.3(66.2)
HF/6-31G(d,p)	38.7(70.7)	40.6(66.5)	39.4(67.1)	−40.6(4.7)	51.5(65.7)
B3LYP/6-31G(d)	16.6(44.5)	18.3(41.1)	17.2(41.8)	−39.1(5.6)	28.7(40.1)
B3LYP/6-31G(d,p)	16.7(43.8)	18.3(40.5)	17.3(41.2)	−39.1(5.6)	28.9(39.5)
MP2/6-31G(d)	12.4(38.5)	14.2(35.3)	13.0(35.8)	−40.7(4.0)	25.2(34.6)
MP2/6-31G(d,p)	12.2(38.1)	14.0(34.9)	12.8(35.5)	−40.9(4.0)	25.0(34.3)
QCISD/6-31G(d)	22.8(54.6)	24.8(50.8)	23.7(51.5)	−40.2(5.2)	35.6(50.0)
CCD/6-31G(d)	22.5(56.3)	24.6(52.7)	23.4(53.3)	−40.9(4.5)	35.6(51.9)

[a] All energy quantities in kcal mol^{-1} and entropies in cal mol^{-1} K^{-1}. The designation "method" implies "method//method" results.

angles listed in Figure 4 indicate that the ring formed by the five heavy atoms in the reacting system becomes close to planar at the TS. The deviation of the ring from planarity increases as the reaction progresses from TS to product: For example, at the MP2/6-31G(d,p) geometry of 4,5-dehydro-1-methyl-1*H*-[1,2,3]triazole, the dihedrals 5-4-3-2 and 3-4-5-1 measure 28.0° and −26.7°, respectively.

The electronic activation energies and activation barriers including zero-point energy corrections, and the standard enthalpies, entropies and Gibbs free energies of activation for the gas-phase 13DC reaction of methyl azide with ethene are collected in Table 3. Values are also listed for the reverse process, namely the gas-phase cycloelimination of ethene from 4,5-dehydro-1-methyl-1*H*-[1,2,3]triazole. These data were calculated using ZPE, $H^{\ominus}$, $S^{\ominus}$, and $G^{\ominus}$ values taken directly the thermochemistry sections of the outputs of GAUSSIAN98 frequency calculations on the reactants, TS and product. As a consequence, our HF/6-31G(d) and B3LYP/6-31G(d) activation enthalpies and entropies are slightly higher and slightly lower, respectively, than those reported by Repasky and Jorgensen,[33] who employed a scaling factor of 0.91 for the vibrational frequencies and treated scaled frequencies under 500 cm^{-1} as classical rotations.

To estimate the error made by treating the internal rotations of the methyl group in methyl azide, in the TS and in the product as vibrations, we attempted to use the undocumented hindered internal rotation analysis option in GAUSSIAN98, mentioned in Ochterski's note on thermochemistry in Gaussian (see http://www.gaussian.com/thermo.htm and ref 48). At the HF/6-31G(d) level of theory, the internal rotation correction to the $H^{\ominus}$ value for methyl azide amounts to 0.3 kcal mol^{-1}, but the correction to $S^{\ominus}$ could not be calculated because, most probably due to a programming error, GAUSSIAN98 reported a negative partition function. Accounting for internal rotation increases $H^{\ominus}$ and $S^{\ominus}$ for the TS by 0.01 kcal mol^{-1} and 0.04 cal mol^{-1} K^{-1}, respectively. When use is made of the B3LYP/6-31G(d) method, the values of $H^{\ominus}$ and $S^{\ominus}$ corrected for internal rotation differ from those used to generate Table 3 by −0.06 kcal mol^{-1} and 0.04 cal mol^{-1} K^{-1}, respectively, for methyl azide, and by 0.01 kcal mol^{-1} and 0.06 cal mol^{-1} K^{-1}, respectively, for the TS. Our attempts to calculate $H^{\ominus}$ and $S^{\ominus}$ values corrected for internal rotation for the product failed with both approaches due to error termination of the corresponding GAUSSIAN98 runs. On the whole, even if incomplete, the results suggest that the proper treatment of the hindered internal rotation of the methyl group is not likely to introduce major changes in the quantities reported in Table 3.

The closest examples to the 13DC reaction of methyl azide with ethene for which experimental kinetic data are available, are the 13DC reactions of substituted phenyl azides to norbornene.[49] In ethyl acetate at 298.25 K, $\Delta^{\ddagger}H^{\ominus}$ has been found to range from 12.5 ± 0.9 kcal mol^{-1} (for a *p*-NO_2 substituent) to 15.0 ± 0.9 kcal mol^{-1} (for a *p*-CH_3 substituent). The smallest and largest $\Delta^{\ddagger}S^{\ominus}$ values measured, −34.9 ± 3.5 cal mol^{-1} K^{-1} and −29.4 ± 3.5 cal mol^{-1} K^{-1}, were in the cases of *p*-NO_2 and *m*-NO_2 substituents, respectively. Thus, the gas-phase MP2 and B3LYP results from Table 3 come close to the experimental findings for similar reactions in solution.

The changes observed in the valence orbitals from SC(8)/6-31G(d,p) calculations along the IRC for the 13DC reaction of methyl azide and ethene are illustrated by Figure 5. The eight orbitals in the middle of the figure were calculated at the MP2/6-31G(d,p) TS geometry, while the orbitals in the top and bottom parts, labeled as "before TS" and "after TS", correspond to geometries along the MP2/6-31G(d,p) minimum energy path, each of which is 12 steps of 0.1 amu$^{1/2}$ bohr away from the TS, in the directions of reactants and product, respectively.

It is relatively straightforward to trace the parentage of the "before TS" SC orbitals back to the reactants. Orbitals ψ_4 and ψ_5 still remain very much engaged in a typical ethene π bond (see, e.g., ref 47), but the distortion of the methyl azide fragment from its equilibrium geometry has already introduced noticeable differences in the shapes of the remaining six orbitals (cf. Figure 3). Orbitals ψ_1 and ψ_6 are responsible for the N−N bond which was described by ψ_1' and ψ_2' in Figure 3. The two π bonds between the central and terminal nitrogens in CH_3N_3 (see Figure 3) have evolved into the bonds realized by the orbital pairs (ψ_2, ψ_3) and (ψ_7, ψ_8). The bonding pattern established between the "before TS" SC orbitals ψ_2, ψ_3, ψ_7, and ψ_8 is complicated, which is demonstrated both by their shapes and overlaps (see Table 4). An attempt to describe the reaction using a six-orbital active space would involve replacing two of the singly occupied orbitals from this quartet by a doubly occupied orbital, orthogonal to all of the active orbitals. Obviously, this would result in a major loss of flexibility within the wave function. As can be seen in Table 5, the "before TS" active-space spin-coupling pattern is strongly dominated by reactant-like Rumer spin eigenfunctions, which couple to singlets the spins of orbitals residing on the same reactant only. Of these, the most important one is (1-6,2-3,4-5,7-8), which is in line with our assignment of orbital pairs to bonding interactions.

The shapes of the SC orbitals at the TS carry more than a hint of the bonding in the product, 4,5-dehydro-1-methyl-1*H*-[1,2,3]triazole. This is particularly evident in the orbitals based on the ethene fragment, ψ_4 and ψ_5. The "before TS" π bond between these orbitals is now almost completely broken, which is also manifested by the decrease of the overlap $\langle\psi_4|\psi_5\rangle$ from 0.676 to 0.250 (see Table 4). At the TS, ψ_4 and ψ_5 are much more engaged in the two new bonds closing the ring, in which their counterparts are orbitals ψ_3 and ψ_6, respectively. The shapes of ψ_3 and ψ_6 suggest that, to be able to interact efficiently with ψ_4 and ψ_5, these orbitals have had to withdraw from their

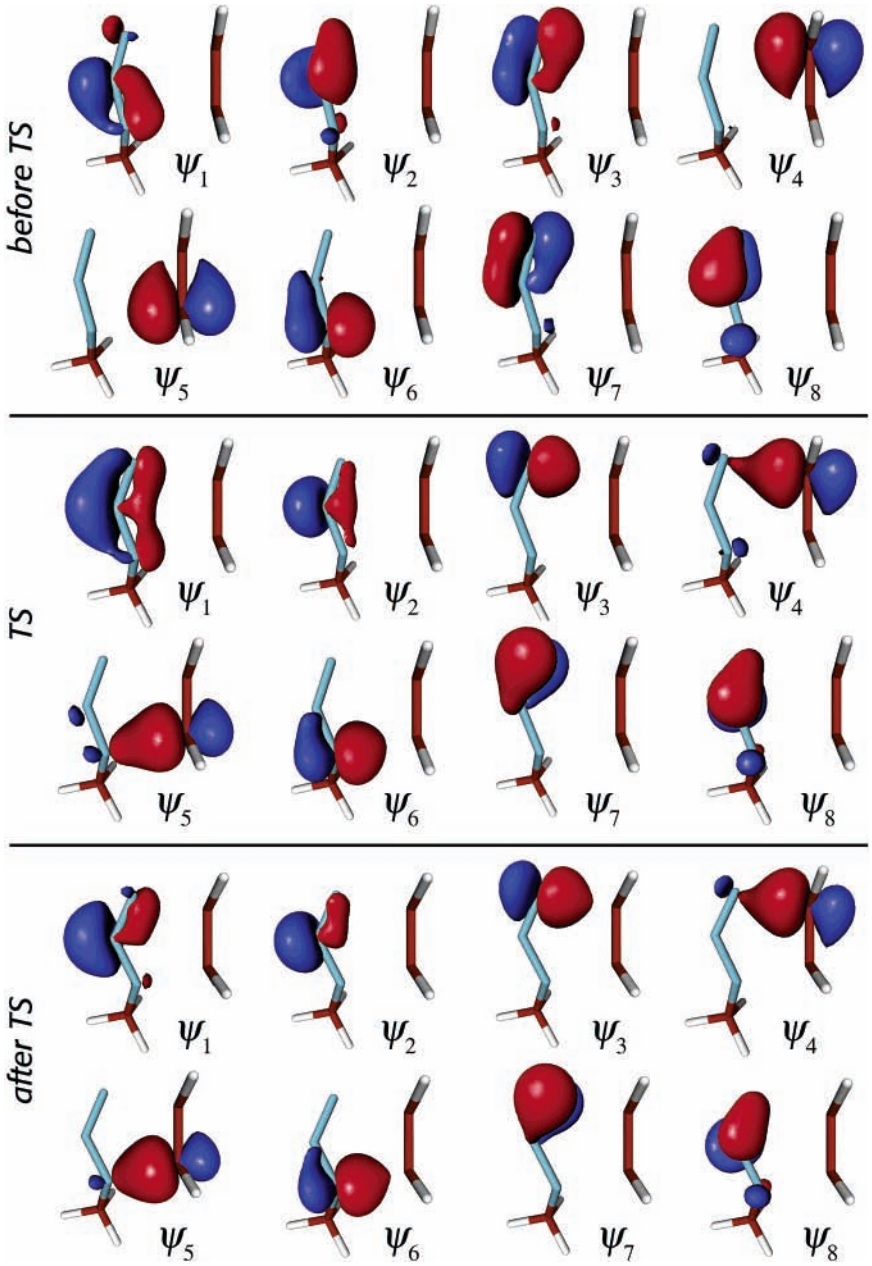

Figure 5. Active (valence) orbitals $\psi_1,\psi_2,...,\psi_8$ from the SC(8)/6-31G(d,p) wave function at different points along the MP2/6-31G(d,p) IRC for the 13DC reaction of methyl azide and ethene. Three-dimensional isovalue surfaces corresponding to $\psi_\mu = \pm 0.1$, drawn from virtual reality modeling language (VRML) files produced by MOLDEN.[46] For further details, see text.

"before TS" partnerships with ψ_2 and ψ_1, respectively. Indeed, the $\langle\psi_1|\psi_6\rangle$ and $\langle\psi_2|\psi_3\rangle$ overlaps are reduced from 0.721 to 0.389, and from 0.532 to 0.272, respectively. Looking at the remaining orbitals, it is not difficult to guess that orbitals ψ_1 and ψ_2 are to become responsible for the lone pair on the central nitrogen in the product, while ψ_7 and ψ_8 now clearly form the almost π component of the N═N bond.

The main contribution to the active-space spin-coupling pattern comes from the first Rumer spin eigenfunction (1-2,3-4,5-6,7-8) (${}^{\mathrm{R}}P_{01}^{8,\mathrm{CC}} = 0.601$, ${}^{\mathrm{R}}P_{01}^{8,\mathrm{GN}} = 0.619$, see Table 5), in which the spins of all pairs of active orbitals which are becoming involved in bonds or in the central nitrogen lone pair in the product are coupled to singlets. Second in importance is the Rumer spin eigenfunction (1-2,3-6,4-5,7-8) (${}^{\mathrm{R}}P_{01}^{8,\mathrm{CC}} = 0.241$; ${}^{\mathrm{R}}P_{01}^{8,\mathrm{GN}} = 0.274$), which, in contrast to the first Rumer spin eigenfunction, is reactant-based: It couples to singlets the spins of the active orbitals that are becoming engaged in the central nitrogen lone pair (ψ_1 and ψ_2), the orbitals that were involved in the ethene π bond (ψ_4 and ψ_5), the orbitals that initially described one of the components of the N≡N bond in methyl azide and later, the almost π component of the N═N bond in the product (ψ_7 and ψ_8), and of the two orbitals which reside on different ends of the 1,3-dipole: ψ_3 and ψ_6. Despite the high overlap between orbitals ψ_2' and ψ_3' in methyl azide ($\langle\psi_2'|\psi_3'\rangle = 0.554$, see Table 1), the six-electron Rumer spin eigenfunction (1-4,2-3,5-6) which couples the spins of the six valence orbitals in this molecule just as they are coupled within the eight-electron Rumer spin eigenfunction for the reacting system (1-2,3-6,4-5,7-8), has a relatively low weight within the overall six-electron active-space spin-coupling pattern (${}^{\mathrm{R}}P_{01}^{6,\mathrm{CC}} = 0.066$, ${}^{\mathrm{R}}P_{01}^{6,\mathrm{GN}} = 0.023$, see Table 2). The weight of spin function (1-2,3-6,4-5,7-8) starts to increase, in parallel with the decrease of the weight of spin function (1-6,2-3,4-5,7-8), as the reactants approach one another and peaks near the TS [at the "before TS" IRC point, it is more informative to consider the Gallup−Norbeck weight of (1-2,3-6,4-5,7-8), see Table 5]. This finding,

TABLE 4: Overlap Integrals $\langle\psi_\mu|\psi_\nu\rangle$ between the SC Orbitals Shown in Figure 5[a]

	ψ_1	ψ_2	ψ_3	ψ_4	ψ_5	ψ_6	ψ_7	ψ_8
		0.479	0.415	0.126	0.267	0.721	-0.433	-0.188
ψ_1	1	0.802	0.470	0.098	0.165	0.389	-0.329	0.154
		0.839	0.345	0.080	0.016	0.166	-0.168	0.427
			0.532	0.110	0.054	0.248	-0.282	0.597
ψ_2		1	0.272	0.210	0.248	0.229	-0.052	0.386
			0.181	0.086	0.089	0.146	0.127	0.514
				0.284	0.217	0.398	-0.818	-0.142
ψ_3			1	0.619	0.089	0.041	-0.150	0.071
				0.625	0.025	-0.050	0.003	0.124
					0.676	0.259	-0.228	-0.059
ψ_4				1	0.250	0.001	-0.035	0.090
					0.254	0.037	-0.011	0.035
						0.326	-0.179	-0.055
ψ_5					1	0.677	-0.001	0.022
						0.696	0.012	-0.024
							-0.388	-0.092
ψ_6						1	-0.067	-0.024
							-0.018	-0.005
								0.424
ψ_7							1	0.553
								0.550
ψ_8								1

[a] The top, middle and bottom values correspond to "before TS", TS, and "after TS" orbitals, respectively.

TABLE 5: Chirgwin−Coulson (${}^{R}P_{0k}^{8,CC}$) and Gallup−Norbeck (${}^{R}P_{0k}^{8,GN}$) Weights of the Rumer Spin Functions Included in the Active-Space Spin-Coupling Pattern Θ_{00}^{8}[a] at Different Points along the MP2/6-31G(d,p) IRC for the 13DC Reaction of Methyl Azide and Ethene

		"before TS"		TS		"after TS"	
k	spin function	${}^{R}P_{0k}^{8,CC}$	${}^{R}P_{0k}^{8,GN}$	${}^{R}P_{0k}^{8,CC}$	${}^{R}P_{0k}^{8,GN}$	${}^{R}P_{0k}^{8,CC}$	${}^{R}P_{0k}^{8,GN}$
1	(1-2,3-4,5-6,7-8)	−0.015	0.001	0.601	0.619	0.865	0.932
2	(1-4,2-3,5-6,7-8)	0.121	0.024	0.034	0.011	−0.003	0.000
3	(1-2,3-6,4-5,7-8)	−0.164	0.091	0.241	0.274	0.070	0.031
4	(1-6,2-3,4-5,7-8)	0.934	0.642	0.007	0.001	−0.006	0.001
5	(1-6,2-5,3-4,7-8)	0.042	0.006	−0.034	0.027	−0.014	0.003
6	(1-2,3-4,5-8,6-7)	−0.004	0.000	0.005	0.000	0.001	0.000
7	(1-4,2-3,5-8,6-7)	0.011	0.001	−0.002	0.000	0.000	0.000
8	(1-2,3-8,4-5,6-7)	0.115	0.072	0.009	0.001	0.005	0.001
9	(1-8,2-3,4-5,6-7)	−0.172	0.055	0.012	0.003	0.002	0.000
10	(1-8,2-5,3-4,6-7)	0.000	0.000	0.003	0.000	0.003	0.000
11	(1-2,3-8,4-7,5-6)	0.020	0.006	0.046	0.028	0.055	0.029
12	(1-8,2-3,4-7,5-6)	−0.012	0.001	−0.001	0.000	0.004	0.000
13	(1-8,2-7,3-4,5-6)	0.017	0.003	0.058	0.027	0.016	0.002
14	(1-8,2-7,3-6,4-5)	0.107	0.098	0.021	0.008	0.002	0.000

[a] See eqs 1 and 2.

in combination with the observed changes in the shapes of the valence orbitals and their overlaps indicates that, on approaching the TS, the bonds realized by the orbital pairs (ψ_1, ψ_6) and (ψ_2, ψ_3) gradually weaken, and that this is accompanied by the formation of a lone pair on the central nitrogen, represented by the singlet-coupled orbitals ψ_1 and ψ_2. As the new bonds involving ψ_3 and ψ_6 are not yet fully developed, the active-space spin function in the vicinity of the TS displays competition (or "resonance") between two spin-coupling patterns: the product-like (1-2,3-4,5-6,7-8) and the reactant-based (1-2,3-6,4-5,7-8). These patterns differ only in the mode of coupling the spins of the four orbitals responsible for the two new bonds closing the ring: ψ_3, ψ_4, ψ_5, and ψ_6. The large separation and low overlap between orbitals ψ_3 and ψ_6 allows us to consider the presence of the less important pattern (1-2,3-6,4-5,7-8), as an indication that the reacting system attains, near the TS, some singlet biradical character. However, there is not even a hint of a benzene-like "resonance" similar to the cases observed near the TS of the Diels−Alder reaction between butadiene and ethene[12] and the TS of the electrocyclization of hexatriene.[24]

The "after-TS" SC picture shows a further development of the product-like features discussed for the TS. The only particularly noticeable changes in the forms of the SC orbitals are some compacting of the lone pair orbitals ψ_1 and ψ_2 (see Figure 5). The active-space spin-coupling pattern is largely dominated by the product-like first Rumer spin eigenfunction (1-2,3-4,5-6,7-8) (${}^{R}P_{01}^{8,CC} = 0.865$, ${}^{R}P_{01}^{8,GN} = 0.932$, see Table 5), while the weight of the reactant-based singlet biradical pattern (1-2,3-6,4-5,7-8) has decreased so much that it is safe to discard its contribution to the overall active-space spin-coupling pattern.

The changes in the shapes of the SC orbitals, in the overlaps between these orbitals and in the composition of the active-

TABLE 6: HF, SC(8), and Full-SCVB(8) Total and Correlation Energies[a] [6-31G(d,p) Basis] for the 13DC Reaction of Methyl Azide with Ethene at Different Points along the MP2/6-31G(d,p) IRC

quantity	"before TS"	TS	"after TS"
E(HF)	−280.84406	−280.84271	−280.87383
E(SC)	−280.96286	−280.95706	−280.98582
E(SCVB)	−280.98625	−280.98219	−281.00276
ΔE^{corr}(SC)	−0.11880 (83.6%)	−0.11435 (82.0%)	−0.11199 (86.9%)
ΔE^{corr}(SCVB)	−0.14219	−0.13948	−0.12893

[a] All energies in hartree.

space spin-coupling pattern give a clear description of the electronic structure changes during the 13DC reaction of methyl azide with ethene. The ethene π bond and two of the three π bonds on the methyl azide fragment break almost simultaneously. This is accompanied by the formation of the two new bonds that close the ring and the formation of the lone pair on the central nitrogen in the reaction product 4,5-dehydro-1-methyl-1*H*-[1,2,3]triazole, all of which also takes place almost in parallel. Throughout the reaction, each SC orbital remains distinctly associated with a single atom while its form, overlap with other SC orbitals and participation in the active-space spin-coupling pattern adjust to accommodate the differences in the nature of the bonding in reactants and product. The bond-breaking and bond-formation processes realized in this way can be illustrated through reaction mechanism D.

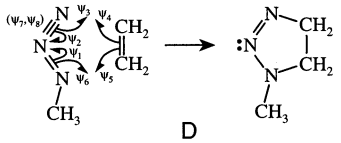

D

This mechanism depicts a homolytic mechanism, which is markedly different from the SC descriptions of other 13DC reactions: The reactions between fulminic acid and ethyne,[10] and between diazomethane and ethene[11] have been found to proceed through heterolytic mechanisms (see reaction mechanisms A1 and B, respectively). While mechanism D appears to have more in common with the homolytic mechanisms resulting from the SC models of the Diels−Alder reaction (see reaction mechanism C and ref 12) and the electrocyclization of hexatriene,[24] there is an important distinction which does not show up in the symbolic half-arrow representations: The reaction paths for both the Diels−Alder reaction and the electrocyclization of hexatriene include conformations, close to the corresponding transition structures, at which the reacting system may be considered aromatic, by virtue of a number of close similarities to the well-known SC description of benzene.[50−52] In contrast, despite the similar homolytic pattern of orbital rearrangements, the $CH_3N_3 + C_2H_4$ reacting system remains decidedly nonaromatic along the whole reaction path.

Formally, the bond described by orbitals ψ_7 and ψ_8 is preserved throughout the reaction. However, the strong interactions between these orbitals and those initially responsible for the other π component of the N≡N bond in CH_3N_3 makes their inclusion in the active space an important factor for maintaining consistency along the reaction path.

The full-SCVB(8) total and correlation energies calculated at the "before TS", TS and "after TS" MP2/6-31G(d,p) IRC points are compared to the corresponding SC(8) quantities in Table 6. The proportion of full-SCVB(8) correlation energy recovered by the SC(8) wave function is not less than 82.0% which is a very good achievement given the fact that it is involves just 14 covalent structures, as opposed to the 1764 covalent and ionic structures within the full-SCVB(8) construction. Still, this percentage is about 10% lower than those normally observed for SC(6) wave functions when studying other pericyclic reactions (see, e.g., refs 10−12 and 24). In search for an explanation, we performed a full-SCVB(6) calculation (including 175 covalent, singly, doubly, and triply ionic structures) for methyl azide using the SC/6-31G(d,p)//MP2/6-31G(d,p) orbitals. The corresponding HF, SC(6), and full-SCVB(6) total energies are −202.86225, −202.94451, and −202.96952 hartree, respectively, and the percentage of full-SCVB(6) correlation energy recovered by the SC(6) wave function turns out to be 76.7%. This is consistent with the amounts of CASSCF correlation energies included in SC descriptions of multiple bonds; for example, the SC(4) construction for the carbon−carbon double bond in ethene captures ca. 77% of the corresponding "4-in-4" CASSCF correlation energy.[47] Thus, the relatively lower amount of full-SCVB(8) correlation energy recovered by the SC(8) wave function along the reaction path for the 13DC reaction of methyl azide with ethene can be attributed to two factors: the presence of a reactant with multiple bonds described within the active space of the SC(8) wave function, and the increased size of the active space, which, in turn, gives rise to a much larger number of structures within the full-SCVB(8) construction.

The additional CASSCF(8,8)/6-31G(d,p)//MP2/6-31G(d,p) calculation at the TS produced a total energy of −280.98386 hartree which, as anticipated, is very close to the corresponding full-SCVB(8) value (see Table 6). This result justifies the use of the full-SCVB(8) wave function as a benchmark for the performance of the much more compact SC(8) ansatz along the path for the 13DC reaction of methyl azide with ethene.

While establishing the SC model for a reaction mechanism, it is usually most convenient to define the SC wave function through eqs 1 and 2 and to analyze the changes in the active-space spin-coupling pattern along the reaction path (for an example, see Table 5 and the associated discussion). Another possibility which places the emphasis on the changes in the resonance pattern between structures, rather than on the recoupling of the spins of the active orbitals, is to use the alternative representation of the SC wave function (9) in conjunction with eq 10. In agreement with the results presented in Table 5, the SC(8)/6-31G(d,p)//MP2/6-31G(d,p) wave function at the TS turns out to be heavily dominated by structures $\Psi^8_{00;1}$(12345678) and $\Psi^8_{00;3}$(12345678), incorporating Rumer spin functions ${}^R\Theta^8_{00;1} \equiv$ (1-2,3-4,5-6,7-8) and ${}^R\Theta^8_{00;3} \equiv$ (1-2,3-6,4-5,7-8), with Chirgwin−Coulson structure occupation numbers of 0.688 and 0.202, respectively (the next largest in magnitude occupation number amounts to 0.046). All covalent structures making up the SC(8) wave function (9) are also present in the full-SCVB(8) construction (7). At the TS, the occupation numbers of these structures add up to 1.167. This shows clearly that the physical picture carried by the full-SCVB(8) wave function is determined by components coming from its SC(8) counterpart and illustrates the difficulties associated with the use of Chirgwin−Coulson structure occupation numbers (the sum of the occupation numbers for all ionic structures has to be a negative number, −0.167). Just as in the SC(8) case, structures $\Psi^8_{00;1}$(12345678) and $\Psi^8_{00;3}$(12345678) are preponderant, with Chirgwin−Coulson structure occupation numbers of 0.834 and 0.248, respectively (the next largest in magnitude occupation number is equal to −0.082). The differences between these occupation numbers and those coming from the SC(8) wave function (see above) can be attributed to the much larger number of nonorthogonal structures appearing in the full-SCVB(8) construction and to

the somewhat arbitrary nature of any weighting expression for a linear combination of nonorthogonal functions, including the Chirgwin−Coulson formula (10).

4. Conclusions

The SC model for the electronic mechanism of the gas-phase 13DC reaction of methyl azide and ethene, presented in this work, shows that not all 13DC reactions proceed through heterolytic bond rearrangements involving movement of well-identifiable orbital pairs that are retained along the entire reaction path from reactants to product, such as those depicted in reaction mechanisms A1 and B. If the bonds within the 1,3-dipole and dipolarophile which break during the reaction are of a low polarity, as in the case of the addition of methyl azide to ethene, then the homolytic mechanism exemplified by reaction mechanism D becomes a viable alternative and we are convinced that the present study by no means exhausts the examples of 13DC reactions adopting a mechanism of this type. Other 13DC reactions which are also very likely to proceed through a homolytic bond rearrangement are those between olefins and other azides (e.g., the well-known 13DC reaction of phenyl azide with norbornene), and between ozone and olefins, a particular example of which, the ozonolysis of ethene, has been discussed by Harcourt.[19]

Neither the heterolytic (see reaction mechanisms A1 and B) nor the homolytic (see reaction mechanism D) SC models for the mechanisms of 13DC reactions involve an aromatic TS. While the heterolytic route is devoid of any significant "resonance", the "resonance" observed along the homolytic pathway suggests that in the vicinity of the TS the reacting system exhibits some singlet biradical character associated with the well-separated orbitals at the two ends of the 1,3-dipole (ψ_3 and ψ_6 in reaction mechanism D).

It should be emphasized that intuition did not play a significant role in setting up the SC calculations described in the present work, or those reported previously for other 13DC reactions, but was limited to choosing the basis set and the number of active orbitals only. The latter sometimes has to be increased slightly, especially if it proves difficult to retain a consistent active space along a reaction pathway, as in the example reported here. In contrast to approaches utilizing closed-shell wave functions and also in contrast to some classical VB schemes, the heterolytic or homolytic nature of the reaction mechanism is not built into the SC wave function. Instead, the wave function is sufficiently flexible to allow both mechanisms: the choice is made by the fully variational procedure used to optimize the core and active orbitals, alongside the active-space spin-coupling pattern. It may come as a surprise that reactions from the same class, such as the 13DC reaction of fulminic acid with ethyne and the 13DC reaction of methyl azide with ethene, are predicted to follow different mechanisms (compare reaction mechanisms A1 and D). However, if one takes into account the differences in the electronic structures of the respective reactants, this makes very good chemical sense.

References and Notes

(1) Huisgen, R. *Angew. Chem.* **1963**, *2*, 565.
(2) Huisgen, R. *J. Org. Chem.* **1976**, *41*, 403.
(3) Firestone, R. *J. Org. Chem.* **1968**, *33*, 2285.
(4) Firestone, R. *Tetrahedron* **1977**, *33*, 3009.
(5) McDouall, J. J. W.; Robb, M. A.; Niazi, U.; Bernardi, F.; Schlegel, H. B. *J. Am. Chem. Soc.* **1987**, *109*, 4642.
(6) Rastelli, A.; Gandolfi, R.; Amadé, M. S. *J. Org. Chem.* **1998**, *63*, 7425.
(7) Borden, W. T.; Loncharich, R. J.; Houk, K. N. *Annu. Rev. Phys. Chem.* **1988**, *39*, 213.
(8) Gerratt, J.; Cooper, D. L.; Karadakov, P. B.; Raimondi, M. *Chem. Soc. Rev.* **1997**, *26*, 87.
(9) Gerratt, J.; Cooper, D. L.; Karadakov, P. B.; Raimondi, M. In *The Encyclopedia of Computational Chemistry*; Schleyer, P. v. R., Ed.; Wiley: New York, 1998; p 2672.
(10) Karadakov, P. B.; Cooper, D. L.; Gerratt, J. *Theor. Chem. Acc.* **1998**, *100*, 222.
(11) Blavins, J. J.; Karadakov, P. B.; Cooper, D. L. *J. Org. Chem.* **2001**, *66*, 4285.
(12) Karadakov, P. B.; Cooper, D. L.; Gerratt, J. *J. Am. Chem. Soc.* **1998**, *120*, 0, 3975.
(13) Leroy, G.; Sana, M.; Burke, L. A.; Nguyen, M. T. In *Quantum Theory of Chemical Reactions*; Daudel, R., Pullman, A., Salem, L., Veillard, A., Eds.; D. Reidel: The Netherlands, 1979; Vol. 1, p 91.
(14) Sana, M.; Leroy, G.; Dive, G.; Nguyen, M. T. *J. Mol. Struct. (THEOCHEM)* **1982**, *89*, 147.
(15) Leroy, G.; Sana, M. *Tetrahedron* **1975**, *31*, 2091.
(16) Leroy, G.; Sana, M. *Tetrahedron* **1976**, *32*, 709.
(17) Nguyen, M. T.; Chandra, A. K.; Sakai, S.; Morokuma, K. *J. Org. Chem.* **1999**, *64*, 65.
(18) Harcourt, R. D. *J. Phys. Chem. A* **2001**, *105*, 10947.
(19) Harcourt, R. D. *J. Mol. Struct.* **1972**, *12*, 351.
(20) Harcourt, R. D.; Schulz, A. *J. Phys. Chem. A* **2000**, *104*, 6510.
(21) Sakata, K. *J. Phys. Chem. A* **2000**, *104*, 10001.
(22) Nguyen, M. T.; Chandra, A. T.; Uchimaru, T.; Sakai, S. *J. Phys. Chem. A* **2001**, *105*, 10947.
(23) Karadakov, P. B.; Cooper, D. L. *J. Phys. Chem. A* **2001**, *105*, 10946.
(24) Karadakov, P. B.; Cooper, D. L.; Thorsteinsson, T.; Gerratt, J. In *Quantum Systems in Chemistry and Physics. Volume 1: Basic Problems and Model Systems*; Hernández-Laguna, A., Maruani, J., McWeeny, R., Wilson, S., Eds.; Kluwer: Dordrecht, 2000; p 327.
(25) Truhlar, D. G.; Kuppermann, A. *J. Am. Chem. Soc.* **1971**, *93*, 1840.
(26) Truhlar, D. G.; Kuppermann, A. *J. Chem. Phys.* **1972**, *56*, 2232.
(27) Fukui, K. *J. Chem. Phys.* **1970**, *74*, 4161.
(28) Fukui, K. In *The World of Quantum Chemistry. Proceedings of the First International Congress of Quantum Chemistry, Menton, 1973*; Daudel, R., Pullman, B., Eds.; D. Reidel: Dordrecht, 1974; p 113.
(29) Andersson, K.; Malqvist, P.-A.; Roos, B. O. *J. Chem. Phys.* **1992**, *96*, 1218.
(30) Hrovat, D. A.; Morokuma, K.; Borden, W. T. *J. Am. Chem. Soc.* **1994**, *116*, 1072.
(31) Kozlowski, P. M.; Dupuis, M.; Davidson, E. R. *J. Am. Chem. Soc.* **1995**, *117*, 774.
(32) Borden, W. T.; Davidson, E. R. *Acc. Chem. Res.* **1996**, *29*, 67.
(33) Repasky, M. P.; Jorgensen, W. L. *Faraday Discuss.* **1998**, *110*, 379.
(34) Frisch, M. J.; Trucks, G. W.; Schlegel, H. B.; Scuseria, G. E.; Robb, M. A.; Cheeseman, J. R.; Zakrzewski, V. G.; J. A. Montgomery, J.; Stratmann, R. E.; Burant, J. C.; Dapprich, S.; Millam, J. M.; Daniels, A. D.; Kudin, K. N.; Strain, M. C.; Farkas, O.; Tomasi, J.; Barone, V.; Cossi, M.; Cammi, R.; Mennucci, B.; Pomelli, C.; Adamo, C.; Clifford, S.; Ochterski, J.; Petersson, G. A.; Ayala, P. Y.; Cui, Q.; Morokuma, K.; Malick, D. K.; Rabuck, A. D.; Raghavachari, K.; Foresman, J. B.; Cioslowski, J.; Ortiz, J. V.; Baboul, A. G.; Stefanov, B. B.; Liu, G.; Liashenko, A.; Piskorz, P.; Komaromi, I.; Gomperts, R.; Martin, R. L.; Fox, D. J.; Keith, T.; Al-Laham, M. A.; Peng, C. Y.; Nanayakkara, A.; Gonzalez, C.; Challacombe, M.; Gill, P. M. W.; Johnson, B.; Chen, W.; Wong, M. W.; Andres, J. L.; Head-Gordon, M.; Replogle, E. S.; Pople, J. A. *Gaussian 98, revision A.7*; Gaussian, Inc.: Pittsburgh, PA, 1998.
(35) Werner, H.-J.; Knowles, P. J.; with contributions from R. D. Amos; Berning, A.; Cooper, D. L.; Deegan, M. J. O.; Dobbyn, A. J.; Eckert, F.; Hampel, C.; Leininger, T.; Lindh, R.; Lloyd, A. W.; Meyer, W.; Mura, M. E.; Nickla, A.; Palmieri, P.; Peterson, K.; Pitzer, R.; Pulay, P.; Rauhut, G.; Schütz, M.; Stoll, H.; Stone, A. J.; Thorsteinsson, T. *MOLPRO (A Package of Ab Initio Programs)*. See: http://www.molpro.net.
(36) Karadakov, P. B.; Gerratt, J.; Cooper, D. L.; Raimondi, M. *J. Chem. Phys.* **1992**, *97*, 7637.
(37) Schmidt, M. W.; Baldridge, K. K.; Boatz, J. A.; Elbert, S. T.; Gordon, M. S.; Jensen, J. H.; Koseki, S.; Matsunaga, N.; Nguyen, K. A.; Su, S. J.; Windus, T. L.; Dupuis, M.; Montgomery, J. A. *J. Comput. Chem.* **1993**, *14*, 1347.
(38) Pauncz, R. *Spin Eigenfunctions*; Plenum Press: New York, 1979.
(39) Karadakov, P. B.; Gerratt, J.; Cooper, D. L.; Raimondi, M. *Theor. Chim. Acta* **1995**, *90*, 51.
(40) Chirgwin, B. H.; Coulson, C. A. *Proc. R. Soc. London, Ser. A* **1950**, *201*, 196.
(41) Gallup, G. A.; Norbeck, J. M. *Chem. Phys. Lett.* **1973**, *21*, 495.
(42) Raimondi, M.; Sironi, M. In *Valence Bond Theory and Chemical Structure*; Klein, D. J., Trinajstić, N., Eds.; Elsevier: Amsterdam, 1990; p 111.

(43) Cooper, D. L.; Gerratt, J.; Raimondi, M.; Wright, S. C. *Chem. Phys. Lett.* **1987**, *138*, 296.
(44) Cooper, D. L.; Gerratt, J.; Raimondi, M.; Wright, S. C. *J. Chem. Soc., Perkin Trans. 2* **1989**, 1187.
(45) Anderson, D. W. W.; Rankin, D. W. H.; Robertson, A. *J. Mol. Struct.* **1972**, *14*, 385.
(46) Schaftenaar, G. *MOLDEN (A Pre- and Postprocessing Program of Molecular and Electronic Structure)*; CAOS/CAMM Center: University of Nijmegen, The Netherlands.
(47) Karadakov, P. B.; Gerratt, J.; Cooper, D. L.; Raimondi, M. *J. Am. Chem. Soc.* **1993**, *115*, 6863.
(48) Ayala, P. Y.; Schlegel, H. B. *J. Chem. Phys.* **1998**, *108*, 2314.
(49) Scheiner, P.; Schomaker, J. H.; Deming, S.; Libbey, W. J.; Nowack, G. P. *J. Am. Chem. Soc.* **1964**, *87*, 306.
(50) Cooper, D. L.; Gerratt, J.; Raimondi, M. *Nature* **1986**, *323*, 699.
(51) Gerratt, J. *Chem. Br.* **1987**, *23*, 327.
(52) Cooper, D. L.; Wright, S. C.; Gerratt, J.; Hyams, P. A.; Raimondi, M. *J. Chem. Soc., Perkin Trans. 2* **1989**, 719.